ACS OMEGA

http://pubs.acs.org/journal/acsodf

Article

Enhancement of Catalytic Activity on Crude Palm Oil Hydrocracking over SiO_2/Zr Assisted with Potassium Hydrogen Phthalate

Hasanudin Hasanudin,* Wan Ryan Asri, Ady Mara, Muhammad Al Muttaqii, Roni Maryana, Nino Rinaldi, Suresh Sagadevan, Qiuyun Zhang, Zainal Fanani, and Fitri Hadiah

Cite This: *ACS Omega* 2023, 8, 20858−20868

Read Online

ACCESS | Metrics & More | Article Recommendations

ABSTRACT: In this study, the catalytic activity of bifunctional SiO_2/Zr catalysts prepared by template and chelate methods using potassium hydrogen phthalate (KHF) for crude palm oil (CPO) hydrocracking to biofuels was investigated. The parent catalyst was successfully prepared by the sol−gel method, followed by the impregnation of zirconium using $ZrOCl_2 \cdot 8H_2O$ as a precursor. The morphological, structural, and textural properties of the catalysts were examined using several techniques, including electron microscopy energy-dispersive X-ray with mapping, transmission electron microscopy, X-ray diffraction, particle size analyzer (PSA), N_2 adsorption−desorption, Fourier transform infrared-pyridine, and total and surface acidity analysis using the gravimetric method. The results showed that the physicochemical properties of SiO_2/Zr were affected by different preparation methods. The template method assisted by KHF (SiO_2/Zr-KHF2 and SiO_2-KHF catalysts) provides a porous structure and high catalyst acidity. The catalyst prepared by the chelate method assisted by KHF (SiO_2/Zr-KHF1) exhibited excellent Zr dispersion toward the SiO_2 surface. The modification remarkably enhanced the catalytic activity of the parent catalyst in the order SiO_2/Zr-KHF2 > SiO_2/Zr-KHF1 > SiO_2/Zr > SiO_2-KHF > SiO_2, with sufficient CPO conversion. The modified catalysts also suppressed coke formation and resulted in a high liquid yield. The catalyst features of SiO_2/Zr-KHF1 promoted high-selectivity biofuel toward biogasoline, whereas SiO_2/Zr-KHF2 led to an increase in the selectivity toward biojet. Reusability studies showed that the prepared catalysts were adequately stable over three consecutive runs for CPO conversion. Overall, SiO_2/Zr prepared by the template method assisted by KHF was chosen as the most prominent catalyst for CPO hydrocracking.

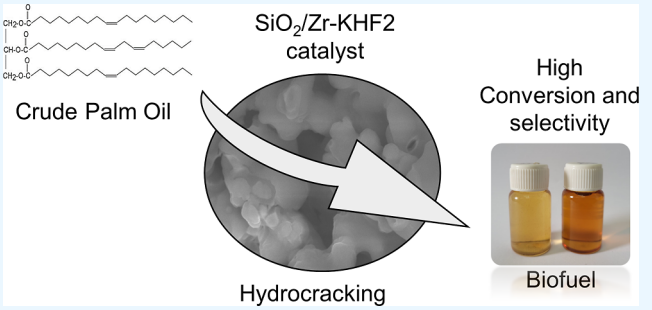

1. INTRODUCTION

Global population expansion has resulted in a decline in the petroleum supply as a vital energy source. This is primarily due to the non-renewable nature of petroleum fuels, which require an extended period for recharge.[1] Worldwide energy consumption has risen in parallel with the expansion of the industrial sector, thus encouraging the necessary exploration of renewable and environmentally acceptable alternative energy sources.[2] Biofuels are among the most intriguing alternative energy sources currently being explored because they are ecofriendly and sustainable. They are broadly extracted from a clean energy source such as vegetable oil which provides non-containing nitrogen and sulfur chemicals.[3] Vegetable oil-based feedstocks consist predominantly of triglycerides, which can be easily transformed into liquid biofuels compared to other existing biomasses.[4] Specifically, Indonesia produces a considerable amount of crude palm oil (CPO) and has an extremely high yield per hectare compared to other vegetable oils. Given its quantity and importance to the Indonesian economy, CPO is both promising and cost-effective as a raw material for manufacturing biofuels. Various energy conversion technologies have been developed to transform triglyceride feedstock into biofuels. Pyrolysis and transesterification are the most commonly used methods for producing biofuels. Nevertheless, when used in engines, the high oxygen content and acidity biofuels produced by the pyrolysis method, as well as other shortcomings produced by the transesterification method, such as high viscosity and low energy content, cause difficulties and are relatively not suitable for long-term production.[5] In these circumstances, the catalytic hydrocracking process provides benefits such as low operational cost, high conversion, and yields toward biofuels.[6] Hydrocracking is a process that involves the successive breaking of

Received: March 8, 2023
Accepted: May 15, 2023
Published: June 1, 2023

© 2023 The Authors. Published by American Chemical Society

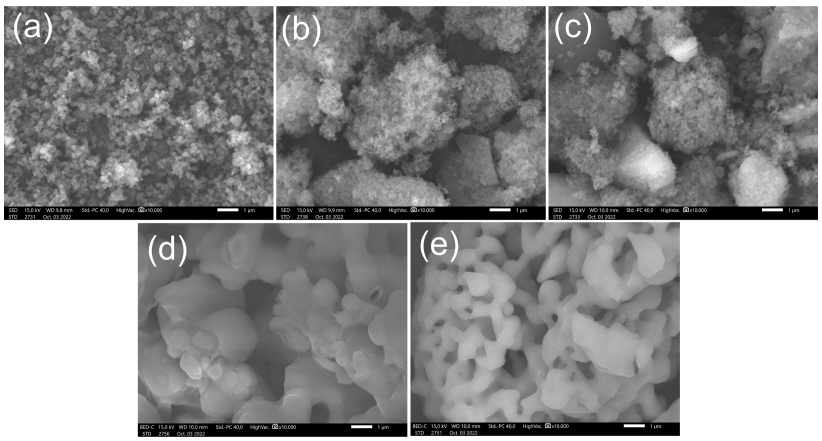

Figure 1. SEM micrographs of (a) SiO_2, (b) SiO_2/Zr, (c) SiO_2/Zr-KHF1, (d) SiO_2/Zr-KHF2, and (e) SiO_2-KHF at 10,000× magnification.

carbon bonds and hydrogenation of bigger hydrocarbon molecules, resulting in smaller ones.[7]

The development of a selective hydrocracking reaction catalyst is critical for ensuring that the process is efficient and profitable. This poses a challenge in producing synthesis processes with controlled features that promote high catalytic activity. Catalysts for hydrocracking processes are typically metal dispersed on the acid support. The metal function involves hydro/dehydrogenation reactions, and in acid supports, the cracking reaction is performed via a bifunctional system.[8] $NiMo/Al_2O_3$ is a commonly utilized conventional hydrotreating catalyst. Bentonites, zeolites, amorphous silica-alumina, mesoporous silica (such as SBA-15 and MCM 41), metal oxides, and mixed oxides have also been investigated.[9]

Particularly, various metal-supported catalysts have been employed for biofuel production through CPO hydroconversion. Subsadsana et al.[10] reported that ZSM-5/MCM-41 loaded with NiMoW promoted conversion up to 62.60 with 9.23% gasoline yield under 2 h reaction at 400 °C for 2 h. Utami et al.[7] reported that the Cr/ZrO_2 catalyst exhibits selectivity toward 65.85% of the gasoline fraction. Among other supports, SiO_2 offers a high specific surface area, excellent thermal stability, and tunable porosity, making it appropriate for the catalyst support.[11] The metal catalysts are often based on noble metals; however, they are exceedingly expensive and susceptible to poisoning and deactivation during their application in hydroconversion reactions.[12] The selection of an adequate non-noble metal-based catalyst for the hydrocracking process is necessary. Various active metals, such as nickel, copper, zirconia, and zinc,[13−15] have been combined with SiO_2 supports. On the other hand, zirconia has been recognized as a comparatively affordable, low toxicity, green, and efficient catalyst for numerous main chemical transformations due to its Lewis acid behavior and high catalytic abilities.[16] Ma et al.[17] discovered that Zr species might improve the acidity characteristics of $MoS_2/SiO_2-Al_2O_2$, resulting in increased catalytic activity for heavy-oil hydrocracking. Another study revealed that the association between Zr loading and catalyst selectivity is consistent with the enhancement of active site formation at the interface between the metal atoms of the Co and Zr promoter species under the SiO_2 support. This catalyst significantly improves propane dehydrogenation compared to the parent Co/SiO_2 catalyst.[18] As a result, there is a compelling motivation for SiO_2/Zr to evaluate its potential as an effective hydrocracking catalyst.

To tune the metal−support interaction, modifications such as morphology, acidity, and structural features of the catalysts are essential aspects that directly affect the catalytic activity. Various additive chemicals have been employed as chelating and templating agents to generate the desired structure.[19−21] Wijaya et al.[22] proposed $NaHCO_3$ as a template for monodisperse hierarchical silica. This method promotes the formation of a $NiMo/SiO_2$ catalyst toward a high liquid product yield in waste frying oil hydrocracking. Ren et al.[23] proposed glycine as a complexing agent to produce a well-dispersed metal-supported Ni/SiO_2 catalyst. Other complexing agents, such as ETDA, citric acid, and ethylene diamine, have been employed to enhance the SiO_2 catalyst by providing excellent catalytic features.[24−26]

In this context, for the first time, potassium hydrogen phthalate (KHF) was employed as a chelating and templating agent for SiO_2/Zr preparation. These methods promote different characteristics that affect the properties of the catalyst as well as the performance of CPO hydrocracking in biofuels. KHF compounds are inexpensive, abundant, and easy to maintain. According to the literature review, neither exploration nor study has been reported yet to compare different preparation methods using KHF as a chelating and templating agent for SiO_2/Zr. The catalyst characteristics were assessed using several techniques. Furthermore, the reusability of the catalyst was evaluated to determine its stability in CPO conversion.

2. RESULTS AND DISCUSSION

2.1. Characterization of Catalysts. Several analyses were conducted to characterize the morphological, structural, and textural properties of the catalysts. Figure 1 depicts the scanning electron microscopy (SEM) micrographs of the parent SiO_2, SiO_2/Zr, and their different modifications involving KHF, that is, the chelating (SiO_2/Zr-KHF1) and templating (SiO_2/Zr-KHF2) methods. It is apparent that the parent SiO_2 (Figure 1a) has a surface morphology with small particles distributed uniformly and exhibits a relative absence of aggregation. After impregnation with Zr (Figure 1b), the surface morphology of SiO_2 tended to agglomerate, indicating the formation of a metal-supported phase. According to Nadia et al.,[22] the formation of agglomerates during the impregnation process suggests that the metal species were successfully loaded onto the supported surface material. The SiO_2/Zr-KHF1 (Figure 1c) catalysts exhibit irregular shapes, suggesting

https://doi.org/10.1021/acsomega.3c01569
ACS Omega 2023, 8, 20858−20868

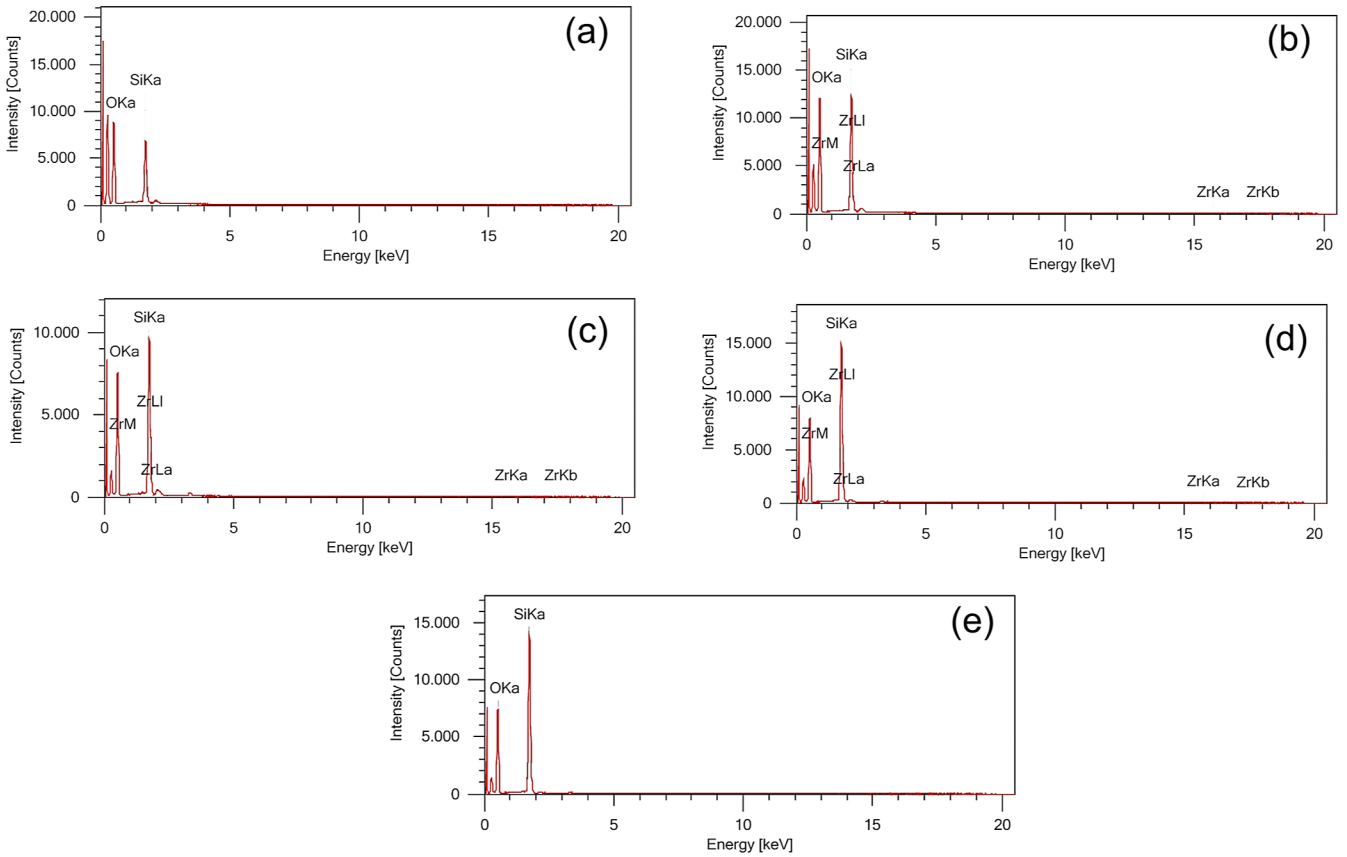

Figure 2. EDX spectra of (a) SiO_2, (b) SiO_2/Zr, (c) SiO_2/Zr-KHF1, (d) SiO_2/Zr-KHF2, and (e) SiO_2-KHF.

Table 1. Elemental Composition of the Catalyst Determined by EDX

	atomic (wt %)				
elements	SiO_2	SiO_2/Zr	SiO_2/Zr-KHF1	SiO_2/Zr-KHF2	SiO_2-KHF
Si	18.21 ± 0.12	22.3 ± 0.10	22.46 ± 0.12	29.35 ± 0.02	30.20 ± 0.13
O	81.75 ± 0.33	77.47 ± 0.27	76.78 ± 0.33	70.36 ± 0.29	69.80 ± 0.30
Zr		0.15 ± 0.02	0.76 ± 0.03	0.29 ± 0.02	

that the chelating agent of KHF randomly increases the dispersion of Zr on the SiO_2 surface. Notably, SiO_2/Zr-KHF2 (Figure 1d) exhibits a different surface morphology compared to SiO_2/Zr-KHF1. SiO_2/Zr prepared by the template method assisted by KHF exhibited a porous surface morphology. In this case, the KHF species were eliminated during calcination, leading to the formation of pores. Similarly, SiO_2-KHF displayed a porous surface morphology but with a more ordered structure.

The energy-dispersive X-ray (EDX) spectra of the modified catalysts and their elemental compositions are shown in Figure 2 and Table 1, respectively. Undoubtedly, the parent SiO_2 and both SiO_2-KHF consisted of Si and O atoms with no impurities, whereas the Zr element was observed in the SiO_2/Zr catalyst, suggesting that the Zr species was successfully incorporated with SiO_2. The Zr content on both modified catalysts prepared by the template and chelate methods varied due to the uneven metal distribution on the SiO_2.[27]

The EDX mapping (Figure 3) shows that the Si and Zr distributions are affected differently depending on the preparation method. Under the chelating method of KHF, Zr is homogeneously distributed toward the SiO_2 surface owing to the strong interaction between the metal and KHF. In this case, the calcination process caused each particle to incline closer. Meanwhile, the templating method caused the catalyst to form an irregular metal distribution. The same elemental distribution feature was also revealed for the parent SiO_2 prepared by the templating methods.

The transmission electron microscopy (TEM) images of the parent SiO_2, SiO_2/Zr, and their modifications using different methods are presented in Figure 4. The parent SiO_2 catalyst (Figure 4a) generally exhibits a spherical particle in nature, whereas semispherical particle agglomerates are formed on the SiO_2/Zr catalyst (Figure 4b). Compared with the parent SiO_2/Zr, the SiO_2/Zr-KHF1 (Figure 4c) shows an increase in tiny black spots, presumably originating from the impregnated species.[28] This suggests that the chelate methods enhance the metal dispersion toward the SiO_2 surface. Distinctive images from SiO_2/Zr-KHF2 (Figure 4d) and SiO_2-KHF were observed because of the preparation of the template method using KHF as an agent. The dark field characteristics with no obvious clear-light patches suggest the presence of a mesoporous structure.[29] Meanwhile, Zr species were not well noticed in the SiO_2/Zr-KHF2. Overall, the TEM image analysis corroborated the SEM−EDX results.

https://doi.org/10.1021/acsomega.3c01569
ACS Omega 2023, 8, 20858−20868

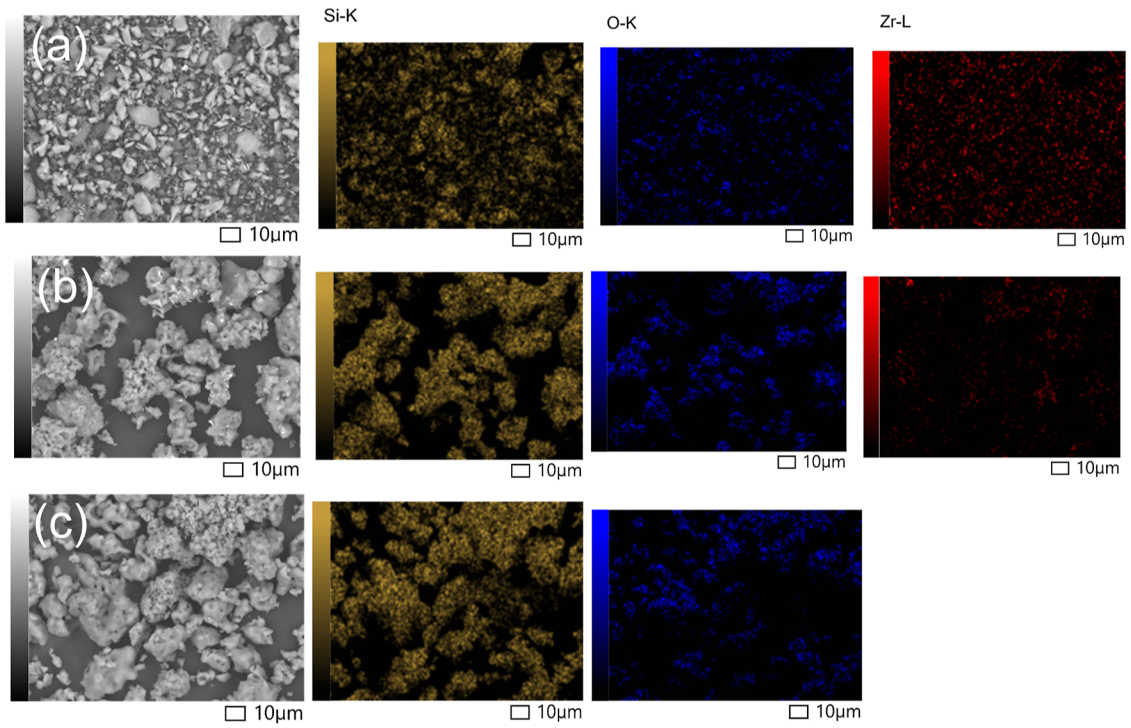

Figure 3. EDX mapping of (a) SiO_2/Zr-KHF1, (b) SiO_2/Zr-KHF2, and (c) SiO_2-KHF.

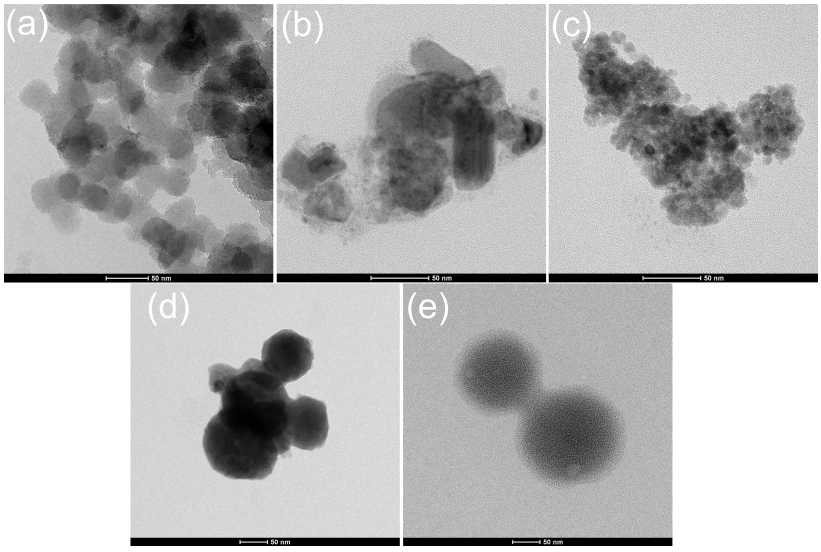

Figure 4. TEM images of (a) SiO_2, (b) SiO_2/Zr, (c) SiO_2/Zr-KHF1, (d) SiO_2/Zr-KHF2, and (e) SiO_2-KHF.

The diffractograms of the parent SiO_2 and SiO_2/Zr and their modifications were assessed to determine the crystal structures of the catalysts. The SiO_2 catalyst (Figure 5a) exhibits a broad diffraction peak 2θ at 22°, suggesting the formation of an amorphous structure.[30] This typical SiO_2 peak is also consistently reported by other studies.[19,31] The diffraction peaks at 2θ = 30, 35.83, 50.28, and 60.08° from SiO_2/Zr (Figure 5b) were ascribed to ZrO_2 with a tetragonal phase (ICDD no. 80-2155).[32] A broad peak was also observed at low 2θ values, indicating that the amorphous silica was retained during impregnation. Meanwhile, no zirconia phase was discerned in SiO_2/Zr-KHF1, indicating good dispersion on the surface of SiO_2, which is presumably less than the detection limit of the X-ray diffraction (XRD).[22] A similar result was also reported by Majewski et al.[33] when preparing the Ni@SiO_2 catalyst, which showed that the unobserved XRD peaks were due to the amorphous phase or the presence of highly dispersed Ni. Furthermore, an appreciable change in the diffractograms can be observed for both SiO_2/Zr-KHF2 and SiO_2-KHF. The 2θ peaks of SiO_2/Zr-KHF2 (Figure 5d) reveal a highly crystalline structure attributed to the formation of quartz and cristobalite mixes that overlapped with the ZrO_2 phases. The template method assisted by KHF (Figure 5e) provides a highly ordered silica structure, thus transforming the amorphous phase into the crystalline phase.

Figure 6 shows the particle size distributions of all the catalysts. The particle size distribution of the parent SiO_2 catalyst (Figure 6a) can be seen to be relatively uniform with a

https://doi.org/10.1021/acsomega.3c01569
ACS Omega 2023, 8, 20858−20868

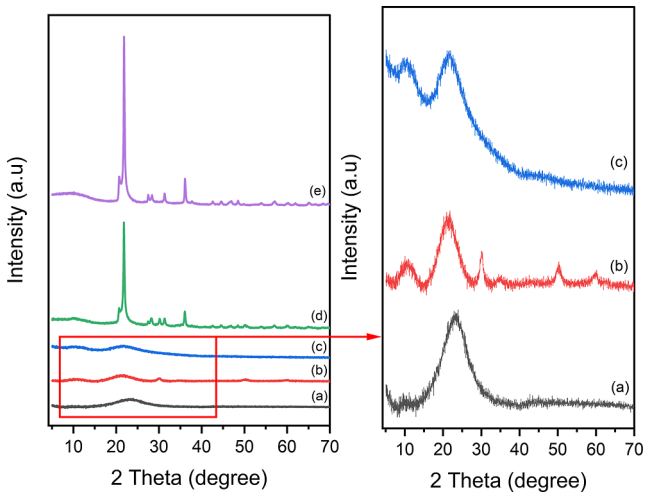

Figure 5. XRD diffractogram of (a) SiO_2, (b) SiO_2/Zr, (c) SiO_2/Zr-KHF1, (d) SiO_2/Zr-KHF2, and (e) SiO_2-KHF.

narrow size distribution, whereas the SiO_2/Zr catalyst (Figure 6b) exhibits a non-uniform particle size distribution owing to the effect of the impregnation process. Gel formation occurs uniformly in the unmodified SiO_2 catalyst because no molecules interfere with gelation. In this case, $Si(OH)_4$ from tetraethyl orthosilicate (TEOS) led to a uniform SiO_2 particle distribution. The SiO_2/Zr-KHF1 catalyst (Figure 6c) showed a particle size distribution similar to that of the parent SiO_2 catalyst, suggesting that the chelating effect of KHF enhanced the particle size distribution of the catalysts. In contrast, the SiO_2/Zr-KHF2 catalyst (Figure 6d) exhibited a wide particle size distribution, suggesting that the template method increased the particle size distribution of the catalysts. The particle size distribution of SiO_2-KHF also revealed properties similar to those of SiO_2/Zr-KHF2 catalysts. When KHF is added during the gelatinization process, KHF interacts with the Si species from TEOS before gel formation so that part of the Si species is bound to four acetate groups while others are bound to KHF, which will eventually change the features of the $Si(OH)_4$ gel, thereby changing the particle size distribution.

The average particle size of the catalysts is listed in Table 2. It is clear that the SiO_2/Zr catalyst exhibited a larger average particle size than the parent SiO_2. This is presumably due to the formation of agglomerated SiO_2 particles.[16] It is apparent that the template method assisted by KHF increased the average particle size relative to the parent SiO_2, whereas it decreased the average particle size of the SiO_2/Zr catalyst. The chelate method assisted by KHF (SiO_2/Zr-KHF1) promoted a decrease in the average particle size of the catalyst, presumably owing to the complex interaction between KHF and Zr.

Table 2. Average Particle Size of Catalysts Determined by PSA

catalysts	average particle size (μm)
SiO_2	22.65 ± 0.35
SiO_2/Zr	49.49 ± 0.04
SiO_2/Zr-KHF1	14.55 ± 0.35
SiO_2/Zr-KHF2	38.61 ± 0.07
SiO_2/KHF	31.49 ± 0.07

The acidity properties of all prepared catalysts are shown in Figure 7. It is noticeable that the parent SiO_2 catalyst had the lowest acidity property from the low Lewis acid sites from Si^{4+} ions.[27] An increase in the total and surface acidity was observed in SiO_2/Zr due to the addition of new Lewis acid sites from Zr^{4+} ions.[34] Furthermore, chelate and template methods assisted by KHF successfully enhanced the acidity of the parent catalysts. The KHF-assisted chelate and template methods successfully enhanced the acidity of the parent

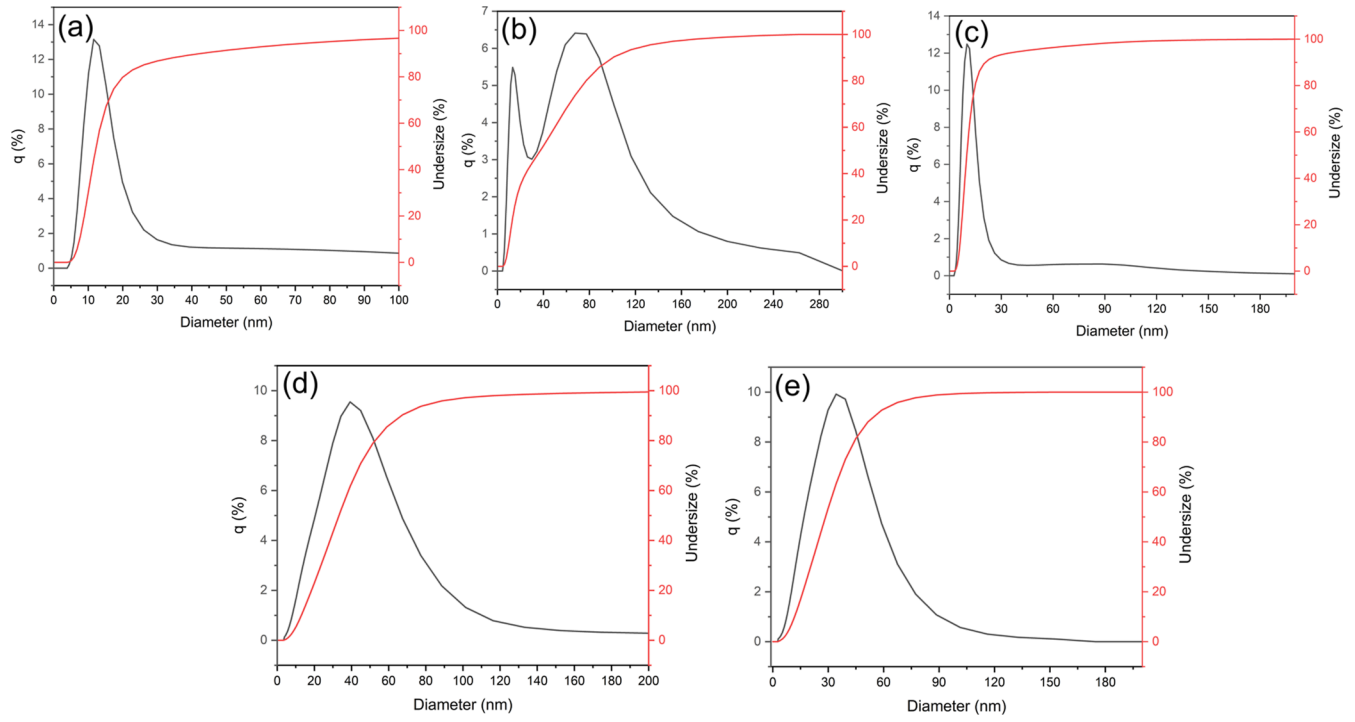

Figure 6. Particle size distribution of (a) SiO_2, (b) SiO_2/Zr, (c) SiO_2/Zr-KHF1, (d) SiO_2/Zr-KHF2, and (e) SiO_2-KHF.

https://doi.org/10.1021/acsomega.3c01569
ACS Omega 2023, 8, 20858−20868

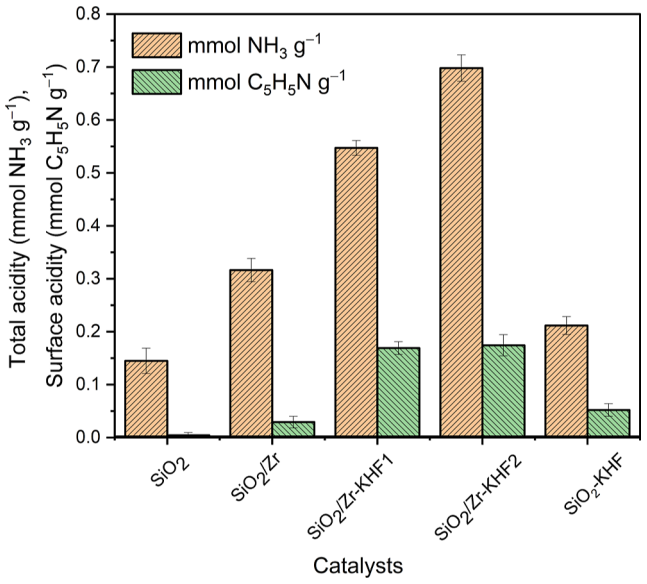

Figure 7. Total and surface acidity of all catalysts determined by the gravimetric methods using NH_3 and C_6H_5N as probes.

catalysts. SiO_2/Zr-KHF2 had a higher total acidity than SiO_2/Zr-KHF1, but the surface acidity remained relatively constant, suggesting the same acidity features on the surface of the catalysts. The pores provided by the template methods might predominantly promote efficient adsorption of the probes toward the acidic sites, thereby increasing the acidity of the catalysts. Similarly, the SiO_2-KHF had a higher total acidity value than the parent SiO_2, suggesting that the pores generated by the KHF template provided efficient base adsorption toward the Si^{4+} sites.

The Fourier transform infrared (FTIR)-pyridine spectra of the catalysts are shown in Figure 8. These spectra distinguish between the Brønsted and Lewis acid sites contained in the catalyst. The absorption peak at ~1625 cm^{-1} is attributed to the presence of Bronsted acid sites from the pyridinium ion.[35] The absorption band at ~1430 cm^{-1} corresponds to coordinated pyridine with Lewis acid sites.[36] It can be seen that the absorption band in both regions increased after the

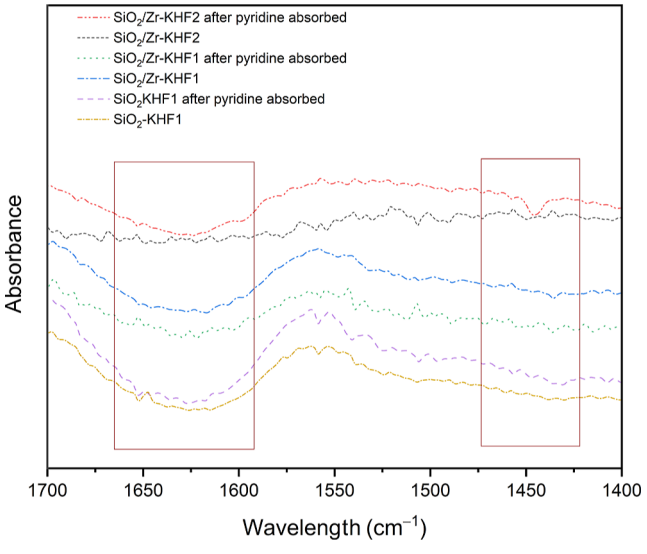

Figure 8. FTIR-pyridine spectra of all catalysts.

adsorption of pyridine by the catalyst. SiO_2/Zr-KHF2 exhibited the highest intensity compared to the other catalysts, which is consistent with the acidity results analyzed by the gravimetric method.

The N_2 physisorption of all the catalysts is shown in Figure 9. It can be seen that all catalysts exhibit a type IV isotherm,

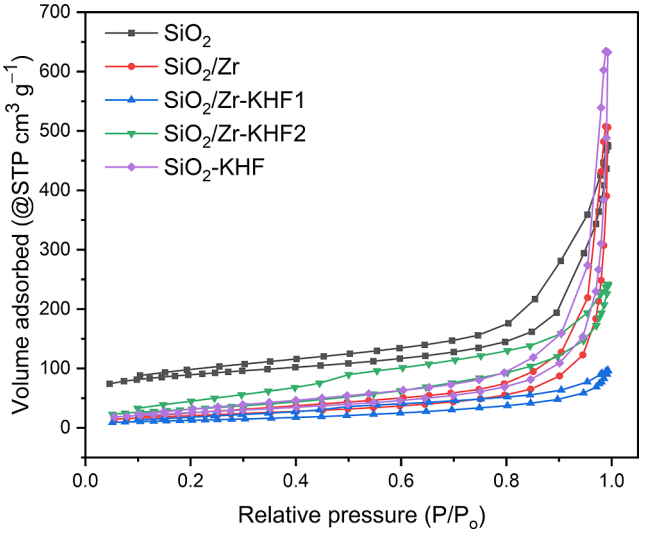

Figure 9. N_2 adsorption desorption of the parent SiO_2 and their modifications using different methods.

indicating a dominant mesoporous material.[37] The H_4 hysteresis was also observed on all catalysts, providing a narrow slit mesopore channel.[38] Sydorchuk et al.[39] stated that this type of loop hysteresis reflects the connectivity of pores of varying sizes, and the material develops noticeable micropores and mesopores. The catalyst's mesoporous characteristic might overcome the inadequate limitation of triglyceride diffusion.[40]

The textural properties of the parent SiO_2 and its modifications are listed in Table 3. The S_{BET} of SiO_2/Zr was

Table 3. Textural Properties of All Catalysts

catalysts	S_{BET} (m^2 g^{-1})	V_p (cc g^{-1})	d (nm)
SiO_2	294	0.73	9.92
SiO_2/Zr	76.43	0.76	39.77
SiO_2/Zr-KHF1	45.35	0.14	12.35
SiO_2/Zr-KHF2	220.5	0.80	14.51
SiO_2-KHF	90.7	0.92	40.57

lower S_{BET} compared with the parent SiO_2 owing to the pore blocking of Zr species.[41] Despite the fact that the SiO_2/Zr-KHF2 prepared by the template method exhibited a decrease in S_{BET}, this method increased the total pore volume (V_p), suggesting an enhancement in the pore features of the catalyst. Conversely, SiO_2/Zr-KHF1 prepared using the chelate method significantly decreased the pore volume. Meanwhile, an appreciable increase in pore diameter (d) in SiO_2-KHF is observed compared with the parent SiO_2 owing to the template-assisted effect of the KHF species, particularly the generation of pores with a high diameter.

2.2. Catalytic Test. The catalytic activities of the parent SiO_2, SiO_2/Zr, and their modifications for CPO hydrocracking are shown in Figure 10. It is recognizable that SiO_2/Zr exhibits a higher conversion (86.37%) than the parent SiO_2 (70.42%)

https://doi.org/10.1021/acsomega.3c01569
ACS Omega 2023, 8, 20858−20868

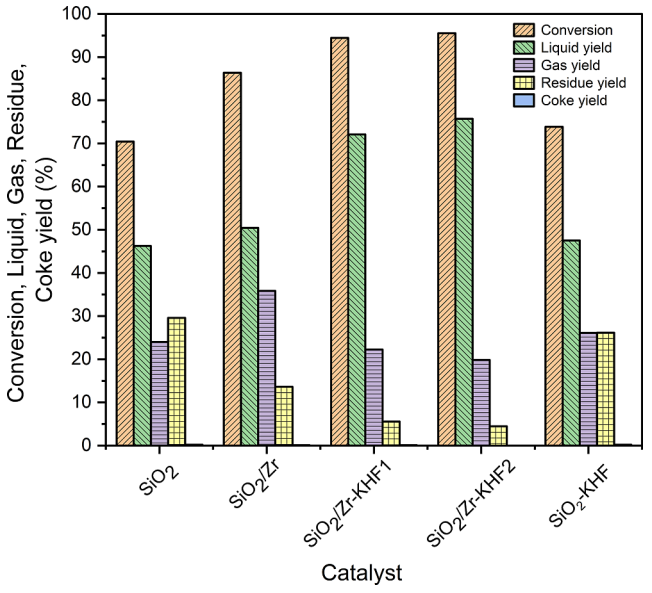

Figure 10. Catalytic activity of CPO hydrocracking over various catalysts.

owing to the presence of Zr Lewis acid sites that promote an increase in the CPO conversion. Similarly, Yongde et al.[42] reported that Zr species could enhance the hydrocracking catalytic activity of $MoS_2/SiO_2-Al_2O_3$—catalysts by increasing the sum of acidic sites. This treatment can improve both the hydrogenation and cracking activities of the bifunctional catalysts. Subsadsana et al.[43] observed the lowest conversion during CPO hydrocracking over ZSM-5, presumably because of the low acidity of the catalyst. The modification of both parent SiO_2 and SiO_2/Zr remarkably enhanced the CPO conversion in the following order: SiO_2/Zr-KHF2 (95.53%) > SiO_2/Zr-KHF1 (94.43%) > SiO_2-KHF (73.83%). This increase in conversion may be correlated with the high acidity of the corresponding catalyst, which is consistent with the results of the acidity measurements. In this respect, the template method using KHF promotes an increase in the acidity of the SiO_2/Zr catalyst compared with the chelate method. SiO_2/Zr-KHF2 promoted effective mass transport as a catalyst because of its efficient mass transport for interaction with the acid sites. Subsadsana et al.[10] reported that the NiMoW-ZSM-5/MCM-41 catalyst exhibits 62.60—71.40% conversion of CPO during 4 h hydrocracking at 400 °C, whereas another study described that the $CoMo/Al_2O_3$ promotes the CPO conversion up to 64.21% under 1 h hydrocracking at 350° and 500 psi.[44]

With regard to the liquid yield, it can be seen that indistinguishable trends are observed in Figure 10, in which the SiO_2/Zr-KHF2 (75.71%) exhibits the highest liquid yield compared with other catalysts. The greater the number of acid sites in the catalytic system, the greater the number of hydrogen radicals acquired and interacted with the feed, and as a consequence, increased the liquid yield.[45] The comparatively high gas yields generated by all catalysts range from 19.82—35.84%, which might be due to high-temperature hydrocracking. The SiO_2/Zr catalyst exhibited the highest gas yield, presumably attributed to successive CPO hydrocracking, leading to an increase in the gas yield. It was observed that both modified SiO_2/Zr-KH1 and SiO_2/Zr-KHF2 successfully promoted the hydrocracking reaction toward a high liquid yield with low residues, suggesting an effective catalyst for the CPO hydrocracking process. It is apparent that the coke yield generated by the parent SiO_2 catalyst decreased after Zr loading from 0.21 to 0.09%. Al-Marshed et al.[46] stated that the presence of metal dispersed could inhibit coke formation due to their hydrogen-transfer reactions. Moreover, the coke yield of SiO_2/Zr continuously decreased after modification by both the template and chelate methods-KHF, but the SiO_2-KHF catalyst remained the same as that of the parent SiO_2. The decreasing order was SiO_2/Zr < SiO_2/Zr-KHF1 < SiO_2/Zr-KHF2, suggesting that the SiO_2/Zr-KHF2 catalyst could effectively suppress the hydrocracking process toward low coke formation.

The effect of various catalysts on product selectivity toward biofuel fractions during CPO hydrocracking is presented in Figure 11. As expected, all catalysts provided different

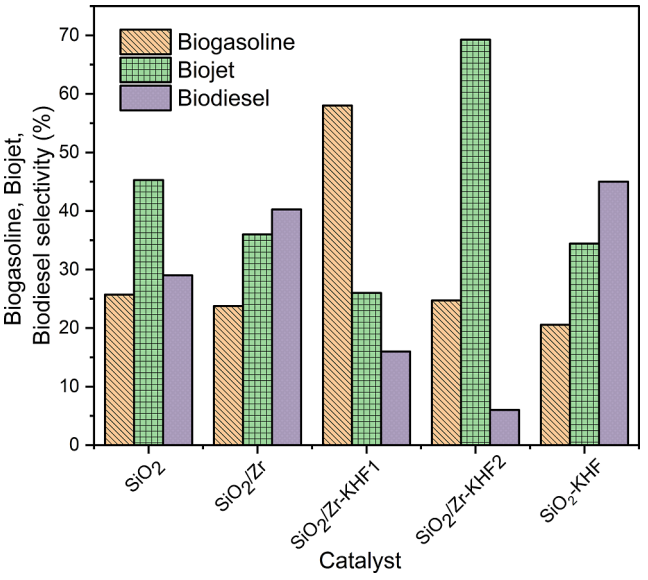

Figure 11. Selectivity results of CPO hydrocracking over various catalysts.

selectivities toward different biofuel fractions. The parent SiO_2 exhibited high selectivity toward biojet (45.28%), whereas the parent SiO_2/Zr promoted high selectivity toward biodiesel (40.25%). The biojet selectivity tends to increase up to 69.27% after modification by the template method (SiO_2/Zr-KHF2) owing to the dominant effect of the mesopore structure. Hydroconversion in the mesopore cavity may hinder the formation of large intermediaries during the hydrocracking process, hence controlling the size of the preferred hydrocarbon molecule selective to the biojet. Meanwhile, SiO_2-KHF dominantly generated a biofuel fraction selectivity toward biodiesel (45.01%) rather than the biojet (45.01%), presumably due to the effect of the porous structure provided by the template method assisted by KHF, thus promoting diffusion effectively. Interestingly, the SiO_2/Zr-KHF catalyst exhibited a higher selectivity toward biogasoline (58%) than the other catalysts. This may be due to the presence of dominant micropores provided by the chelate method assisted by the KHF catalyst.

Table 4 shows the catalytic activity of various catalysts during palm oil hydrocracking. It can be seen that the SiO_2/Zr modified by KHF using the chelate and template method exhibits an adequate performance during CPO hydroconversion compared with other reported catalysts (Table 4)

https://doi.org/10.1021/acsomega.3c01569
ACS Omega 2023, 8, 20858—20868

Table 4. Comparison of Catalytic Activity Using Various Catalysts on Palm Oil Hydrocracking

catalyst	reaction condition	results	references
zeolite Y	batch reactor, mass ratio of palm oil to catalyst = 20:1, T = 390°C	conversion = ca. 70 wt %, $Y_{bio\text{-}jet}$ = 42 wt %, $S_{hydrocarbon}$ = 91%	47
NiW-HY	batch reactor, T = 400°C, for 120 min, H_2 flow rate = 500 cm^3 min^{-1}, P = 3 MPa for 30 min	conversion = 50.38%, $Y_{biogasoline}$ = 13.88%, $Y_{biokerosene}$ = 18.20%, $Y_{biodiesel}$ = 18.30%	48
Ni-SAPO-34	batch reactor, mass ratio of palm oil tocatalysts = 20:1, T = 390°C for 8 h, P = 3 MPa	conversion = 97.5%, $Y_{bio\text{-}jet}$ = 42.03%, S_{alkene} = 65%, S_{arene}= 11%	49
NiW-HZSM-5	batch reactor, T = 400°C, t = 120 min, H_2 flow rate = 500 cm^3 min^{-1}, P = 3 MPa for 30 min	conversion = 48.18%, $Y_{biogasoline}$ = 10.44%, $Y_{biokerosene}$ = 19.56%, $Y_{biodiesel}$ = 18.22%	48
Pd−Fe	batch reactor, palm oil = 100 mL, catalyst loading = 0.9 g, T = 400°C for 2 h, P = 60 bar	conversion = 94%, $S_{gasoline}$ = 62.20%, $S_{kerosene}$ = 31.71%, S_{diesel} = 6.63%, Y_{diesel} = 62.20%, $Y_{kerosene}$ = 31.71%	40
MoN/bentonite	continuous fixed bed reactor, T = 458°C for 0.12 h, mass ratio of palm oil to catalyst = 0.12 w/w, flow rate palm oil = 11.94 g min^{-1}, H_2 flow rate = 2 mL min^{-1}	conversion = 78.33%, Y_{liquid} = 50.32%, Y_{gas} = 44%, biogasoline fraction = 28.7%, bioaviation fraction = 15.69%	3
$CoMo/Al_2O_3$	batch reactor, T = 350°C for 1 h, P = 500 psi	conversion = 64.21 wt %, Y_{liquid} = 90.56 wt %, Y_{gas} = 8.98 wt %	44
SiO_2/Zr-KHF1	continuous fixed bed reactor, catalyst weight = 0.5 g, CPO flow rate = 20 mL h^{-1}, T = 500°C	conversion = 94.43%, $S_{biogasoline}$ = 58%, S_{biojet} = 26%, $S_{biodiesel}$ = 16%, Y_{liquid} = 72.08%	this work
SiO_2/Zr-KHF2	continuous fixed bed reactor, catalyst weight = 0.5 g, CPO flow rate = 20 mL h^{-1}, T = 500°C	conversion = 95.53%, $S_{biogasoline}$ = 24.72%, S_{biojet} = 69.27%, $S_{biodiesel}$ = 6.01%, Y_{liquid} = 75.71%	this work
SiO_2-KHF	continuous fixed bed reactor, catalyst weight = 0.5 g, CPO flow rate = 20 mL h^{-1}, T = 500°C	conversion = 73.83%, $S_{biogasoline}$ = 20.56%, S_{biojet} = 34.43%, $S_{biodiesel}$ = 45.01%, Y_{liquid} = 47.52%	this work

with high conversion and liquid yield and promotes high selectivity toward biogasoline and biojet.

The reusability of the catalysts was assessed in three consecutive runs to evaluate their stability in the conversion of CPO. The spent catalyst was washed with hexane (50 mL), heated at 105 °C for 1 h, and subsequently subjected to heat treatment, including calcination at 850 °C for 3 h with an O_2 flow rate of 30 mL h^{-1} and reduction at 600 °C for 3 h with a H_2 flow rate of 30 mL h^{-1}. As shown in Figure 12, generally, all

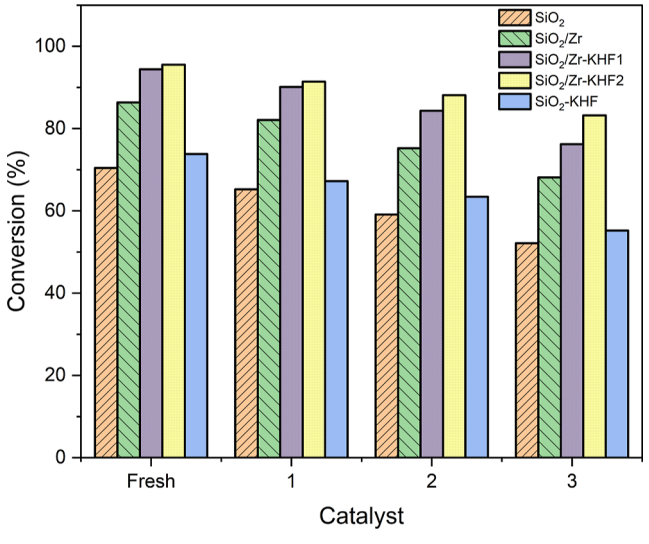

Figure 12. Reusability performance of all catalysts on CPO conversion.

catalysts showed a decrease in the catalytic performance, and a prolonged decrease was observed after three consecutive runs. This is due to the heavy product deposition on the catalyst, such as coke, which blocks the active sites of the catalyst.[3,42]

Compared to the parent catalyst, a relatively insignificant decrease was observed for SiO_2/Zr-KHF2, followed by the SiO_2/Zr-KHF1 catalyst, suggesting that the modified catalyst could inhibit coke formation. Further analysis of coke yield on the spent catalyst emphasizes this notion. Based on Table 5,

Table 5. Coke Yield of Spent Catalysts

	coke yield (%)		
catalysts	1st	2nd	3rd
SiO_2	0.21	0.51	1.03
SiO_2/Zr	0.09	0.32	0.83
SiO_2/Zr-KHF1	0.073	0.28	0.44
SiO_2/Zr-KHF2	0.001	0.10	0.35
SiO_2-KHF	0.21	0.32	0.67

SiO_2 exhibited the highest increase in coke yield after a series of consecutive runs, suggesting a decrease in the catalytic performance. Meanwhile, the modified catalyst showed an insignificant increase in coke yield, with SiO_2/Zr-KHF2 showing the lowest coke yield after three consecutive runs. The modification of SiO_2/Zr using KHF as a templating agent successfully enhanced the properties of the catalyst, which inherently promoted hydrocracking catalytic activity toward high CPO conversion.

3. CONCLUSIONS

In this study, bifunctional SiO_2/Zr catalysts were synthesized by chelating and templating methods using KHF and were employed for hydrocracking CPO to biofuels. The physicochemical features of the parent and modified catalysts were assessed by several procedures including SEM−EDX with mapping, TEM, XRD, PSA, N_2 adsorption−desorption, FTIR-pyridine, and total and surface acidity analysis using the gravimetric method. The empirical results revealed that the modification of the parent SiO_2 and SiO_2/Zr with both the template and chelate methods assisted by KHF significantly promoted CPO conversion and liquid products in the order SiO_2-KHF > SiO_2/Zr-KHF1 > SiO_2/Zr-KHF2. Moreover, the difference in the preparation method using KHF also showed different catalyst properties that directly affected the catalytic activity toward a particular biofuel selectivity. SiO_2/Zr-KHF2 predominantly promoted selectivity toward high bio-jet, whereas SiO_2/Zr-KHF1 promoted selectivity toward biogasoline. Furthermore, a reusability study showed that the modified

https://doi.org/10.1021/acsomega.3c01569
ACS Omega 2023, 8, 20858−20868

catalysts were appreciably stable during the three reaction cycles and suppressed coke formation.

4. MATERIALS AND METHODS

4.1. Materials. TEOS [$Si(OC_2H_5)_4$, 98%], ammonia solution (NH_4OH, 28%), ethanol (CH_3OH, ≥99.5), KHF ($C8H_5KO_4$ ≥99.95%), zirconium(IV) oxide chloride octahydrate ($ZrOCl_2{\cdot}8H_2O$, ≥97.0%), and pyridine (C_5H_5N, ≥99.9%) were obtained from Sigma-Aldrich without further purification.

4.2. Preparation of SiO_2 Assisted with KHF as a Templating Agent. Briefly, 25 mL of TEOS was diluted with 50 mL of ethanol and stirred for 15 min at ambient temperature. Subsequently, 16.5 mL of KHF solution (10% w/v) was introduced and stirred for 3 h at ambient temperature, followed by gradual dripping of 2 mL of ammonia solution. Subsequently, the solution was aged at ambient temperature for 30 min and then dried at 85 °C for 1 day. The 60-mesh powder was calcined at 850 °C for 3 h at an O_2 flow rate of 30 mL h^{-1}, and the resulting powder was denoted as SiO_2-KHF. The catalyst was then washed with DI water and centrifuged at 3500 rpm for 10 min until the pH was close to neutral. The solution was heated until the water evaporated and then dried at 120 °C for 1 day. A SiO_2 catalyst, without the addition of KHF, was also prepared as a control.

4.3. Synthesis of SiO_2/Zr Assisted with KHF as a Templating Agent. The as-prepared SiO_2-KHF described earlier was mixed with 200 mL of zirconium(IV) oxide chloride (0.04 mol L^{-1}) and stirred for 1 h at ambient temperature. Furthermore, the temperature was moderately increased to 85 °C, and the mixture was stirred for 3 h until a paste was formed. The paste was subsequently heated at 120 °C for 3 h, calcined at 850 °C for 3 h with an O_2 flow rate of 30 mL h^{-1}, and reduced at 600 °C for 3 h with an H_2 flow rate of 30 mL h^{-1}. The catalyst is denoted as SiO_2/Zr KHF2. A SiO_2/Zr catalyst, without the addition of KHF, was also prepared as a control.

4.4. Synthesis of SiO_2/Zr Assisted with KHF as a Chelating Agent. Briefly, 20 mL of ethanol was reacted with 25 μL of TEOS with stirring for 15 min at ambient temperature. Next, 2.578 g of zirconium(IV) oxide chloride powder and a KHF solution (16.5 mL) were mixed and added to the previously prepared solution and stirred for 3 h. Subsequently, 2 mL of the ammonia solution was gradually dripped. The solution was aged at ambient temperature for 30 min and then dried at 85 °C for 1 day. The 60-mesh powder was calcined at 850 °C for 3 h at an O_2 flow rate of 30 mL h^{-1}, and the resulting powder was denoted as SiO_2/ZrO_2-KHF. Next, the catalyst was washed with DI water and centrifuged at 3500 rpm for 10 min until the pH closed to neutral. The solution was heated until the water evaporated and followed by drying at 120 °C for 1 day. The powder was subsequently calcined at 850 °C for 3 h at an O_2 flow rate of 30 mL h^{-1} and reduced at 600 °C for 3 h at an H_2 flow rate of 30 mL h^{-1}. The catalyst is denoted as SiO_2/Zr-KHF1.

4.5. Catalyst Characterization. SEM micrographs equipped with EDX were recorded using a JSM-IT200A/LA, JEOL (acceleration voltage of 20.00 kV and magnification of 10,000 times). TEM images were obtained using the Tecnai G2 20S-Twin function. A Rigaku Smart Lab X-ray powder diffractometer was used to analyze the diffractograms of the catalysts. The particle size distribution and average particle size of the catalysts were determined using a Horiba Partica LA-960 instrument. The measurements were calculated using the static light scattering method (0.01 to 5000 μm). The total and surface acidity were assessed using the gravimetric methods with ammonia and pyridine as probes, as reported by others.[50] The catalyst containing pyridine was directly analyzed using an FT1R-8201PC infrared spectrophotometer (Shimadzu) to determine the acidic sites of the catalyst. The textural properties of the catalysts were analyzed by N_2 adsorption−desorption using NOVA Quantachrome at 77.35 K. The catalyst was outgassed at 275 °C prior to analysis. The surface area of the catalyst (S_{BET}) was determined using the Brunauer−Emmett−Teller (BET) multiplot method, whereas the properties of the catalyst pore were calculated by the Barrett−Joyner−Halenda method.

4.6. Catalytic Activity Test. A continuous system microcylindrical reactor was utilized to conduct the hydrocracking process with 0.5 g of the catalyst. The CPO feed with a flow rate of 20 mL h^{-1} was injected into the reactor using a syringe pump. Hydrocracking was carried out at 500 °C for 1 h under a hydrogen atmosphere at a flow rate of 30 mL h^{-1}. The liquid product was analyzed using GC−MS (Thermo Scientific, TG-5MS column). The temperature was increased (5 °C min^{-1}) from 50 °C for 3 min to 300 °C for 10 min. The flow rate of helium as the carrier gas was 1 mL min^{-1}. Data analysis of the hydrocracking results was performed according to the following equations

$$\text{conversion (\% wt)} = \frac{\text{CPO feed (g)} - \text{residue (g)}}{\text{CPO feed (g)}} \times 100\% \quad (1)$$

$$Y_{\text{liquid}}\ (\%\ \text{wt}) = \frac{\text{liquid product (g)}}{\text{CPO feed (g)}} \times 100\% \quad (2)$$

$$Y_{\text{coke}}\ (\%\ \text{wt}) = \frac{\text{coke (g)}}{\text{CPO feed (g)}} \times 100\% \quad (3)$$

$$Y_{\text{residue}}\ (\%\ \text{wt}) = \frac{\text{residue (g)}}{\text{CPO feed (g)}} \times 100\% \quad (4)$$

$$Y_{\text{gas}}\ (\%\ \text{wt}) = 100\%\ \text{wt} - (Y_{\text{liqud product}} + Y_{\text{coke}} + Y_{\text{residue}}) \quad (5)$$

$$S_{\text{liquid product}}\ (\%) = \frac{\%\ \text{GCMS biofuel fraction area}}{\%\ \text{GCMS total area}} \times 100\% \quad (6)$$

AUTHOR INFORMATION

Corresponding Author

Hasanudin Hasanudin − *Department of Chemistry, Faculty of Mathematics and Natural Science, Universitas Sriwijaya, Indralaya, Sumatra Selatan 30662, Indonesia; Biofuel Research Group, Faculty of Mathematics and Natural Science, Universitas Sriwijaya, Indralaya, Sumatra Selatan 30662, Indonesia;* orcid.org/0000-0003-2153-9163; Phone: +6281367471272; Email: hasanudin@mipa.unsri.ac.id

https://doi.org/10.1021/acsomega.3c01569
ACS Omega 2023, 8, 20858−20868

Authors

Wan Ryan Asri − *Chemistry Department, King Fahd University of Petroleum and Minerals, Dhahran 31261, Saudi Arabia*

Ady Mara − *Department of Chemistry, Faculty of Mathematics and Natural Science, Universitas Sriwijaya, Indralaya, Sumatra Selatan 30662, Indonesia; Biofuel Research Group, Faculty of Mathematics and Natural Science, Universitas Sriwijaya, Indralaya, Sumatra Selatan 30662, Indonesia*

Muhammad Al Muttaqii − *Research Center for Chemistry, Indonesian Institute of Sciences, Tangerang Selatan, Banten 15314, Indonesia*

Roni Maryana − *Research Center for Chemistry, Indonesian Institute of Sciences, Tangerang Selatan, Banten 15314, Indonesia*

Nino Rinaldi − *Research Center for Chemistry, Indonesian Institute of Sciences, Tangerang Selatan, Banten 15314, Indonesia*

Suresh Sagadevan − *Nanotechnology & Catalysis Research Centre, Universiti Malaya, Kuala Lumpur 50603, Malaysia*

Qiuyun Zhang − *School of Chemistry and Chemical Engineering, Anshun University, Anshun, Guizhou 561000, China;* orcid.org/0000-0002-3905-962X

Zainal Fanani − *Department of Chemistry, Faculty of Mathematics and Natural Science, Universitas Sriwijaya, Indralaya, Sumatra Selatan 30662, Indonesia*

Fitri Hadiah − *Department of Chemical Engineering, Faculty of Engineering, Universitas Sriwijaya, Indralaya 30662, Indonesia*

Complete contact information is available at: https://pubs.acs.org/10.1021/acsomega.3c01569

Notes

The authors declare no competing financial interest.

■ ACKNOWLEDGMENTS

The authors gratefully acknowledge DRPM Ministry of Education, Culture, Research and Technology, Indonesia, for funding this research through PDUPT research grant SPPK no. 059/E5/PG.02.00.PL/2023.

■ REFERENCES

(1) Sari, E. P.; Wijaya, K.; Trisunaryanti, W.; Syoufian, A.; Hasanudin, H.; Saputri, W. D. The Effective Combination of Zirconia Superacid and Zirconia-Impregnated CaO in Biodiesel Manufacturing: Utilization of Used Coconut Cooking Oil (UCCO). *Int. J. Energy Environ. Eng.* **2022**, *13*, 967−978.

(2) Hasanudin, H.; Asri, W. R.; Purwaningrum, W.; Riyanti, F.; Novia, N.; Maryana, R.; Muttaqii, M. A. Kinetic Parameters Investigation for The Esterification of Free Fatty Acid from Coconut Oil Mill Waste Using Montmorillonite-Sulfonated Carbon from Glucose Composite Catalyst. *Molekul* **2022**, *17*, 355−364.

(3) Hasanudin, H.; Asri, W. R.; Said, M.; Hidayati, P. T.; Purwaningrum, W.; Novia, N.; Wijaya, K. Hydrocracking Optimization of Palm Oil to Bio-Gasoline and Bio-Aviation Fuels Using Molybdenum Nitride-Bentonite Catalyst. *RSC Adv.* **2022**, *12*, 16431−16443.

(4) Ahmad, M.; Farhana, R.; Raman, A. A. A.; Bhargava, S. K. Synthesis and Activity Evaluation of Heterometallic Nano Oxides Integrated ZSM-5 Catalysts for Palm Oil Cracking to Produce Biogasoline. *Energy Convers. Manage.* **2016**, *119*, 352−360.

(5) Burimsitthigul, T.; Yoosuk, B.; Ngamcharussrivichai, C.; Prasassarakich, P. Hydrocarbon Biofuel from Hydrotreating of Palm Oil over Unsupported Ni−Mo Sulfide Catalysts. *Renewable Energy* **2021**, *163*, 1648−1659.

(6) Taufiqurrahmi, N.; Bhatia, S. Catalytic Cracking of Edible and Non-Edible Oils for the Production of Biofuels. *Energy Environ. Sci.* **2011**, *4*, 1087−1112.

(7) Utami, M.; Safitri, R.; Fajar Pradipta, M.; Wijaya, K.; Woong Chang, S.; Ravindran, B.; Ovi, D.; Rajabathar, J. R.; Poudineh, N.; Moonsamy Gengan, R. Enhanced Catalytic Conversion of Palm Oil into Biofuels by Cr-Incorporated Sulphated Zirconia. *Mater. Lett.* **2022**, *309*, 131472.

(8) Amaya, J.; Suarez, N.; Moreno, A.; Moreno, S.; Molina, R. Mo or W Catalysts Promoted with Ni or Co Supported on Modified Bentonite for Decane Hydroconversion. *New J. Chem.* **2020**, *44*, 2966−2979.

(9) Badoga, S.; Sharma, R. V.; Dalai, A. K.; Adjaye, J. Hydrotreating of Heavy Gas Oil on Mesoporous Zirconia Supported NiMo Catalyst with EDTA. *Fuel* **2014**, *128*, 30−38.

(10) Subsadsana, M.; Sansuk, S.; Ruangviriyachai, C. Enhanced Liquid Biofuel Production from Crude Palm Oil over Synthesized NiMoW-ZSM-5/MCM-41 Catalyst. *Energy Sources, Part A* **2018**, *40*, 237−243.

(11) Alisha, G. D.; Trisunaryanti, W.; Syoufian, A. Hydrocracking of Waste Palm Cooking Oil into Hydrocarbon Compounds over Mo Catalyst Impregnated on SBA-15. *Silicon* **2022**, *14*, 2309−2315.

(12) Gonçalves, V. O. O.; de Souza, P. M.; Cabioc'h, T.; da Silva, V. T.; Noronha, F. B.; Richard, F. Hydrodeoxygenation of M-Cresol over Nickel and Nickel Phosphide Based Catalysts. Influence of the Nature of the Active Phase and the Support. *Appl. Catal., B* **2017**, *219*, 619−628.

(13) Yao, L.; Shi, J.; Xu, H.; Shen, W.; Hu, C. Low-Temperature CO2 Reforming of Methane on Zr-Promoted Ni/SiO2 Catalyst. *Fuel Process. Technol.* **2016**, *144*, 1−7.

(14) Lomate, S.; Sultana, A.; Fujitani, T. Effect of SiO2 Support Properties on the Performance of Cu-SiO2 Catalysts for the Hydrogenation of Levulinic Acid to Gamma Valerolactone Using Formic Acid as a Hydrogen Source. *Catal. Sci. Technol.* **2017**, *7*, 3073−3083.

(15) Giniyatova, S.; Dauletbekova, A.; Baimukhanov, Z.; Vlasukova, L.; Akilbekov, A.; Usseinov, A.; Kozlovskiy, A.; Akylbekova, A.; Seitbayev, A.; Karipbayev, Z. Structure, Electrical Properties and Luminescence of ZnO Nanocrystals Deposited in SiO2/Si Track Templates. *Radiat. Meas.* **2019**, *125*, 52−56.

(16) Hasanudin, H.; Asri, W. R.; Fanani, Z.; Adisti, S. J.; Hadiah, F.; Maryana, R.; Al Muttaqii, M.; Zhu, Z.; Machado, N. T. Facile Fabrication of SiO2/Zr Assisted with EDTA Complexed-Impregnation and Templated Methods for Crude Palm Oil to Biofuels Conversion via Catalytic Hydrocracking. *Catalysts* **2022**, *12*, 1522.

(17) Wu, Y. J.; Zhang, W. T.; Yang, M. M.; Zhao, Y. H.; Liu, Z. T.; Yan, J. Y. Cobalt Supported on Zr-Modified SiO2 as an Efficient Catalyst for Fischer-Tropsch Synthesis. *RSC Adv.* **2017**, *7*, 24157−24162.

(18) Zhao, Y.; Sohn, H.; Hu, B.; Niklas, J.; Poluektov, O. G.; Tian, J.; Delferro, M.; Hock, A. S. Zirconium Modification Promotes Catalytic Activity of a Single-Site Cobalt Heterogeneous Catalyst for Propane Dehydrogenation. *ACS Omega* **2018**, *3*, 11117−11127.

(19) Wijaya, K.; Saputri, W. D.; Aziz, I. T. A.; Wangsa; Heraldy, E.; Hakim, L.; Suseno, A.; Utami, M. Mesoporous Silica Preparation Using Sodium Bicarbonate as Template and Application of the Silica for Hydrocracking of Used Cooking Oil into Biofuel. *Silicon* **2022**, *14*, 1583−1591.

(20) Bian, Z.; Xin, Z.; Meng, X.; Tao, M.; Lv, Y. H.; Gu, J. Effect of Citric Acid on the Synthesis of CO Methanation Catalysts with High Activity and Excellent Stability. *Ind. Eng. Chem. Res.* **2017**, *56*, 2383−2392.

(21) Ran, R.; Guo, Y.; Zheng, Y.; Wang, K.; Shao, Z. Well-Crystallized Mesoporous Samaria-Doped Ceria from EDTA-Citrate Complexing Process with in Situ Created NiO as Recyclable Template. *J. Alloys Compd.* **2010**, *491*, 271−277.

(22) Nadia, A.; Wijaya, K.; Falah, I. I.; Sudiono, S.; Budiman, A. Self-Regeneration of Monodisperse Hierarchical Porous NiMo/Silica Catalyst Induced by NaHCO3 for Biofuel Production. *Waste Biomass Valorization* **2022**, *13*, 2335−2347.
(23) Ren, H.; Ding, S.; Ma, Q.; Song, W.; Zhao, Y.; Liu, J.; He, Y.; Tian, S. The Effect of Preparation Method of Ni-Supported SiO2 Catalysts for Carbon Dioxide Reforming of Methane. *Catalysts* **2021**, *11*, 1221.
(24) Kaplin, I. Y.; Lokteva, E. S.; Golubina, E. V.; Lunin, V. V. Template Synthesis of Porous Ceria-Based Catalysts for Environmental Application. *Molecules* **2020**, *25*, 4242.
(25) Li, W.; Zhao, Z.; Ding, F.; Guo, X.; Wang, G. Syngas Production via Steam-CO2 Dual Reforming of Methane over LA-Ni/ZrO2 Catalyst Prepared by l -Arginine Ligand-Assisted Strategy: Enhanced Activity and Stability. *ACS Sustainable Chem. Eng.* **2015**, *3*, 3461−3476.
(26) Zhang, Q.; Long, K.; Wang, J.; Zhang, T.; Song, Z.; Lin, Q. A Novel Promoting Effect of Chelating Ligand on the Dispersion of Ni Species over Ni/SBA-15 Catalyst for Dry Reforming of Methane. *Int. J. Hydrogen Energy* **2017**, *42*, 14103−14114.
(27) Wijaya, K.; Nadia, A.; Dinana, A.; Pratiwi, A. F.; Tikoalu, A. D.; Wibowo, A. C. Catalytic Hydrocracking of Fresh and Waste Frying Oil over Ni-and Mo-Based Catalysts Supported on Sulfated Silica for Biogasoline Production. *Catalysts* **2021**, *11*, 1150.
(28) Hauli, L.; Wijaya, K.; Armunanto, R. Preparation and Characterization of Sulfated Zirconia from a Commercial Zirconia Nanopowder. *Orient. J. Chem.* **2018**, *34*, 1559−1564.
(29) Hartati; Trisunaryanti, W.; Mukti, R. R.; Kartika, I. A.; Firda, P. B. D.; Sumbogo, S. D.; Prasetyoko, D.; Bahruji, H. Highly Selective Hierarchical ZSM-5 from Kaolin for Catalytic Cracking of Calophyllum Inophyllum Oil to Biofuel. *J. Energy Inst.* **2020**, *93*, 2238−2246.
(30) Putri, Q. U.; Hasanudin, H.; Asri, W. R.; Mara, A.; Maryana, R.; Gea, S.; Wijaya, K. Production of Levulinic Acid from Glucose Using Nickel Phosphate - Silica Catalyst. *React. Kinet., Mech. Catal.* **2023**, *136*, 287−309.
(31) Wijaya, K.; Lammaduma Malau, M. L.; Utami, M.; Mulijani, S.; Patah, A.; Wibowo, A. C.; Chandrasekaran, M.; Rajabathar, J. R.; Al-Lohedan, H. A. Synthesis, Characterizations and Catalysis of Sulfated Silica and Nickel Modified Silica Catalysts for Diethyl Ether (DEE) Production from Ethanol towards Renewable Energy Applications. *Catalysts* **2021**, *11*, 1511.
(32) Sakti La Ore, M.; Wijaya, K.; Trisunaryanti, W.; Saputri, W. D.; Heraldy, E.; Yuwana, N. W.; Hariani, P. L.; Budiman, A.; Sudiono, S. The Synthesis of SO4/ZrO2and Zr/CaO Catalysts via Hydrothermal Treatment and Their Application for Conversion of Low-Grade Coconut Oil into Biodiesel. *J. Environ. Chem. Eng.* **2020**, *8*, 104205.
(33) Majewski, A. J.; Wood, J.; Bujalski, W. Nickel-Silica Core@shell Catalyst for Methane Reforming. *Int. J. Hydrogen Energy* **2013**, *38*, 14531−14541.
(34) Hasanudin, H.; Asri, W. R.; Putri, Q. U.; Fanani, Z.; Agustina, T. E.; Wijaya, K. Montmorillonite-Zirconium Phosphate Catalysts for Methanol Dehydration. *Iran. J. Catal.* **2022**, *12*, 389−397.
(35) Hasanudin, H.; Asri, W. R.; Zulaikha, I. S.; Ayu, C.; Rachmat, A.; Riyanti, F.; Hadiah, F.; Zainul, R.; Maryana, R. Hydrocracking of Crude Palm Oil to a Biofuel Using Zirconium Nitride and Zirconium Phosphide-Modified Bentonite. *RSC Adv.* **2022**, *12*, 21916−21925.
(36) Bokade, V.; Moondra, H.; Niphadkar, P. Highly Active Brønsted Acidic Silicon Phosphate Catalyst for Direct Conversion of Glucose to Levulinic Acid in MIBK−Water Biphasic System. *SN Appl. Sci.* **2020**, *2*, 51.
(37) Bian, Z.; Deng, S.; Sun, Z.; Ge, T.; Jiang, B.; Zhong, W. Multi-Core@Shell Catalyst Derived from LDH@SiO2 for Low- Temperature Dry Reforming of Methane. *Renewable Energy* **2022**, *200*, 1362−1370.
(38) Ye, R. P.; Gong, W.; Sun, Z.; Sheng, Q.; Shi, X.; Wang, T.; Yao, Y.; Razink, J. J.; Lin, L.; Zhou, Z.; Adidharma, H.; Tang, J.; Fan, M.; Yao, Y. G. Enhanced Stability of Ni/SiO2 Catalyst for CO2 Methanation: Derived from Nickel Phyllosilicate with Strong Metal-Support Interactions. *Energy* **2019**, *188*, 116059.
(39) Sydorchuk, V.; Janusz, W.; Khalameida, S.; Skwarek, E.; Skubiszewska-Zięba, J.; Leboda, R.; Zazhigalov, V. Synthesis, Structure and Some Properties of Zirconium Phosphate/Oxide Support Compositions. *J. Therm. Anal. Calorim.* **2012**, *108*, 1009−1016.
(40) Srihanun, N.; Dujjanutat, P.; Muanruksa, P.; Kaewkannetra, P. Biofuels of Green Diesel− Kerosene−Gasoline Production from Palm Oil : Effect of Palladium Cooperated with Second Metal on Hydrocracking Reaction. *Catalysts* **2020**, *10*, 241.
(41) Hasanudin, H.; Asri, W. R.; Andini, L.; Riyanti, F.; Mara, A.; Hadiah, F.; Fanani, Z. Enhanced Isopropyl Alcohol Conversion over Acidic Nickel Phosphate-Supported Zeolite Catalysts. *ACS Omega* **2022**, *7*, 38923−38932.
(42) Ma, Y.; Liang, R.; Wu, W.; Zhang, J.; Cao, Y.; Huang, K.; Jiang, L. Enhancing the Activity of MoS2/SiO2-Al2O3 Bifunctional Catalysts for Suspended-Bed Hydrocracking of Heavy Oils by Doping with Zr Atoms. *Chin. J. Chem. Eng.* **2021**, *39*, 126−134.
(43) Subsadsana, M.; Sangdara, P.; Ruangviriyachai, C. Effect of Bimetallic NiW Modified Crystalline ZSM-5 Zeolite on Catalytic Conversion of Crude Palm Oil and Identification of Biofuel Products. *Asia-Pac. J. Chem. Eng.* **2017**, *12*, 147−158.
(44) Tye, C. T.; Looi, P. Y.; Meow, T. L. Hydroprocessing of Crude Palm Oil to Bio-Diesel Using Mesoporous Catalysts. *Adv. Mater. Res.* **2012**, *560*−*561*, 538−543.
(45) Wijaya, K.; Kurniawan, M. A.; Saputri, W. D.; Trisunaryanti, W.; Mirzan, M.; Hariani, P. L.; Tikoalu, A. D. Synthesis of Nickel Catalyst Supported on ZrO2/SO4pillared Bentonite and Its Application for Conversion of Coconut Oil into Gasoline via Hydrocracking Process. *J. Environ. Chem. Eng.* **2021**, *9*, 105399.
(46) Al-Marshed, A.; Hart, A.; Leeke, G.; Greaves, M.; Wood, J. Effectiveness of Different Transition Metal Dispersed Catalysts for In Situ Heavy Oil Upgrading. *Ind. Eng. Chem. Res.* **2015**, *54*, 10645−10655.
(47) Basir, N. M.; Jamil, N. A. M.; Hamdan, H. Conversion of Jet Biofuel Range Hydrocarbons from Palm Oil over Zeolite Hybrid Catalyst. *Nanomater. Nanotechnol.* **2021**, *11*, 184798042098153.
(48) Subsadsana, M.; Ruangviriyachai, C. Effect of NiW Modified Hzsm-5 and HY Zeolites on Hydrocracking Conversion of Crude Palm Oil to Liquid Hydrocarbons. *Orient. J. Chem.* **2016**, *32*, 839−844.
(49) Li, T.; Cheng, J.; Huang, R.; Yang, W.; Zhou, J.; Cen, K. Hydrocracking of Palm Oil to Jet Biofuel over Different Zeolites. *Int. J. Hydrogen Energy* **2016**, *41*, 21883−21887.
(50) Kurnia Amin, A.; Wijaya, K.; Trisunaryanti, W. The Catalytic Performance of ZrO2-SO4 and Ni/ZrO2-SO4 Prepared from Commercial ZrO2 in Hydrocracking of LDPE Plastic Waste into Liquid Fuels. *Orient. J. Chem.* **2018**, *34*, 3070−3078.

https://doi.org/10.1021/acsomega.3c01569
ACS Omega 2023, 8, 20858−20868